Journal of Microbiology (2013) Vol. 51, No. 5, pp. 639–643
DOI 10.1007/s12275-013-3412-2

Experimental Phasing Using Zinc and Sulfur Anomalous Signals Measured at the Zinc Absorption Peak

Sangmin Lee[1,2], Min-Kyu Kim[1], Chang-Jun Ji[3], Jin-Won Lee[3*], and Sun-Shin Cha[1,2,4*]

[1]*Marine Biotechnology Research Division, Korea Institute of Ocean Science and Technology, Ansan 426-744, Republic of Korea*
[2]*Ocean Science and Technology School, Korea Maritime University, Pusan 606-791, Republic of Korea*
[3]*Department of Life Science and Institute for Natural Sciences, Hanyang University, Seoul 133-791, Republic of Korea*
[4]*Department of Marine Biotechnology, University of Science and Technology, Daejeon 305-333, Republic of Korea*

(Received July 31, 2013 / Accepted August 27, 2013)

Iron is an essential transition metal required for bacterial growth and survival. Excess free iron can lead to the generation of reactive oxygen species that can cause severe damage to cellular functions. Cells have developed iron-sensing regulators to maintain iron homeostasis at the transcription level. The ferric uptake regulator (Fur) is an iron-responsive regulator that controls the expression of genes involved in iron homeostasis, bacterial virulence, stress resistance, and redox metabolism. Here, we report the expression, purification, crystallization, and phasing of the apo-form of *Bacillus subtilis* Fur (*Bs*Fur) in the absence of regulatory metal ions. Crystals were obtained by microbatch crystallization method at 295 K and diffraction data at a resolution of 2.6 Å was collected at the zinc peak wavelength (λ=1.2823 Å). Experimental phasing identified the positions of one zinc atom and four sulfur atoms of cysteine residues coordinating the zinc atom, indicating that the data contained a meaningful anomalous scattering originating from the ordered zinc-coordinating sulfur atoms, in spite of the small anomalous signals of sulfur atoms at the examined wavelength.

Keywords: Ferric uptake regulator, transcription regulator, crystallization, experimental phasing

Introduction

Iron is an indispensable metal required for bacterial growth and survival. It serves as a cofactor for diverse enzymes implicated in tricarboxylic acid cycle, respiration, gene regulation, and DNA synthesis. It contributes to the structural integrity of proteins (Hernandez *et al*., 2002). However, excess free iron in the bacterial cytosol is potentially toxic under aerobic conditions because of its ability to catalyze the formation of reactive oxygen species (ROS) via Fenton or Haber-Weiss reactions (Haber and Weiss, 1932). To maintain the delicate balance of iron concentration, bacteria have developed highly sensitive iron-responsive transcription regulators that control the expression of genes involved in iron uptake and storage machinery in response to iron availability (Berg and Shi, 1996; Escolar *et al*., 1999; Schaible and Kaufmann, 2004).

Fur (ferric uptake regulator) is a representative iron-sensing transcription regulator in bacteria. Under iron-rich conditions, the ferrous ions bind to Fur, and the fully coordinated form of Fur (holo-Fur) recognizes DNA sequences called Fur boxes (Kadner, 2005; Dian *et al*., 2011), regulating the expression of target genes. In addition, Fur plays an important role in the transcriptional modulation of bacterial virulence, acid resistance, nitrosative/oxidative resistance, and redox metabolism (McHugh *et al*., 2003; Palyada *et al*., 2004; Gancz *et al*., 2006; Lee and Helmann, 2007; da Silva Neto *et al*., 2009; Torres *et al*., 2010).

According to the available crystal structures of Fur family proteins (*Pseudomonas aeruginosa* Fur (*Pa*Fur) (Pohl *et al*., 2003), *Bacillus subtilis* PerR (*Bs*PerR) (Traore *et al*., 2006), *Vibrio cholerae* Fur (*Vc*Fur) (Sheikh and Taylor, 2009), *Helicobacter pylori* Fur (*Hp*Fur) (Dian *et al*., 2011), and *Campylobacter jejuni* Fur (*Cj*Fur) (Butcher *et al*., 2012), Fur adopts a modular architecture consisting of N-terminal DNA-binding domain (DB), a C-terminal dimerization domain (D-domain) that mediates Fur dimerization, and a hinge region connecting the two domains. The Fur proteins have two or three metal-binding sites per monomer. The first metal site (C-site) is located close to the carboxyl terminus and consists of four conserved cysteine residues in two Cys-X-X-Cys motifs. The second metal site (M-site), located at the interface between DB- and D-domains, is constructed by the residues from the hinge region, DB-domain, and D-domain. The residues from the D-domain and hinge region form the D-site, which is adjacent to M-site (Pohl *et al*., 2003; Dian *et al*., 2011; Shin *et al*., 2011).

Fur belongs to the Fur family, which includes sensors of Fe (Ferric uptake regulator, Fur), Zn(II) (Zinc uptake regulator, Zur), Ni(II) (Nickel uptake regulator, Nur), Mn(II) (Manganese uptake regulator, Mur), and hydrogen peroxide (Peroxide-sensing protein, PerR) (Lee and Helmann, 2007). Although each of the Fur subfamilies sense distinct metals and recognize different DNA sequences, they share the overall structure as well as the metal-binding sites. Structural and biochemical studies of Fur family proteins revealed the functional roles of the three metal sites. The M-site has been established as a primary regulatory site whose allosteric binding

*For correspondence. (S.-S. Cha) E-mail: chajung@kiost.ac; Tel.: +82-31-400-6297; Fax: +82-31-406-2495 / (J.-W. Lee) E-mail: jwl@hanyang.ac.kr; Tel.: +82-2-2220-0952; Fax: +82-2-2299-3495

with Fur proteins is required for DNA binding (Sheikh and Taylor, 2009; Dian *et al.*, 2011; Shin *et al.*, 2011; Ma *et al.*, 2012). The D-site has been proposed to be a secondary regulatory site that is non-essential for DNA binding, but which modulates the DNA-binding affinity of Fur family proteins (Dian *et al.*, 2011; Shin *et al.*, 2011; Ma *et al.*, 2012). The C-site is a structural zinc-binding site, which maintains the structural integrity of Fur proteins (Traore *et al.*, 2006; Dian *et al.*, 2011; Shin *et al.*, 2011; Ma *et al.*, 2012).

According to the classical activation model of Fur proteins, Fur proteins with regulatory metal ions bind to the promoter regions of target genes. However, some biochemical and spectroscopic analyses showed that apo-Fur proteins without regulatory metal ions can bind to its target DNA sequences and modulate their transcription (Delany *et al.*, 2001a, 2001b; Lee *et al.*, 2007; Dian *et al.*, 2011; Butcher *et al.*, 2012). In spite of extensive structural studies about Fur proteins, structural information on this family has been restricted to holo-Fur proteins. The crystal structure of *Cj*Fur with its C- and D-sites occupied by zinc was recently reported. Although a *Cj*Fur structure with empty M-sites was proposed to offer an insight into the apo-state of Fur proteins (Butcher *et al.*, 2012), it is not compatible with the transcriptional activity of apo-Fur, because the recognition helix, which plays critical roles in DNA recognition, is positioned outside the DNA-binding site in this structure. Here, we report the over-expression, crystallization, preliminary X-ray crystallographic analyses, and experimental phasing of apo-*Bs*Fur with empty D- and M-sites as the first step toward structure determination. The crystal structure of apo-Fur without regulatory metal ions will extend an invaluable opportunity for the structural elucidation of the iron-independent DNA-binding activities of apo-Fur proteins.

Materials and Methods

Expression, purification, and crystallization of *Bs*Fur

*Bs*Fur exhibits 33%, 32%, 34%, 23%, and 33% sequence identities to *Pa*Fur, *Bs*PerR, *Vc*Fur, *Hp*Fur, and *Cj*Fur, respectively. The *BsFur* gene (GenBank accession No. 938727) was amplified from the *B. subtilis* genomic DNA by using two primers, fur-F (5′-AAACATATGGAAAACCGTATTGATCG-3′) and fur-R (5′-CTCGGATCCGTCTATTCAGTTTCTTTTCCG-3′). The amplified gene was digested by *Nde*I and *Bam*HI, and inserted downstream of the T7 promoter of the expression plasmid pET-11a (+) vector (Novagen, USA). The resulting construct in pET-11a contained residues 1–149 of the *Bs*Fur protein with no additional residue. After verifying the DNA sequence, the plasmid DNA was transformed into *Escherichia coli* strain BL21(DE3) pLysS (Promega Corp., USA). The cells were grown to an optical density (OD_{600}) of ~0.5 in Luria-Bertani medium (Merck, USA) containing 50 μg/ml ampicillin at 310 K and the expression was induced by 1 mM isopropyl-β-D-1-thiogalactopyranoside (IPTG; Duchefa, USA). After a 4-h-long induction at 310 K, the cells were harvested and re-suspended in 20 mM Tris-HCl (pH 8.0) containing 5% glycerol and 10 mM EDTA. The cells were disrupted by sonication and the cell debris was discarded after centrifugation at 20,000×*g* for 30 min at 277 K. The resulting supernatant was loaded onto a 20-ml Heparin Sepharose™ column (GE Healthcare, Sweden). The column

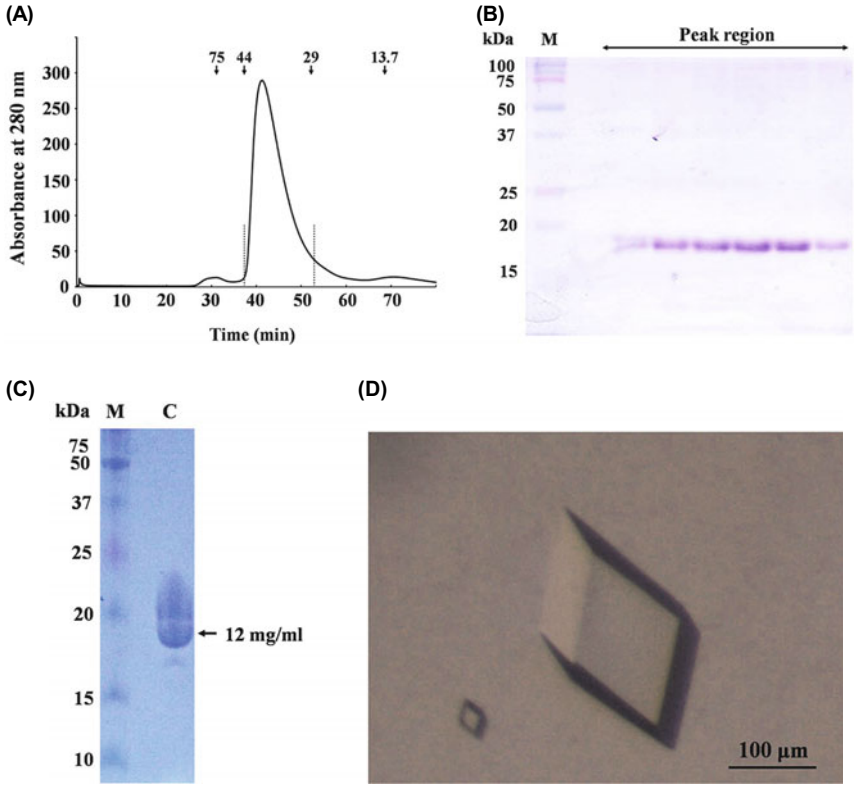

Fig. 1. Purification and crystallization of apo-*Bs*Fur. (A) Elution profile of size-exclusion chromatography (SEC). The peak region used for crystallization is indicated by two dotted lines. Here, 75, 44, 29, and 13.7 represent the elution points of standard size markers with molecular weights of 75, 44, 29, and 13.7 kDa, respectively. (B) Coomassie blue-stained 12% SDS-PAGE gel of the SEC peak region collected in 1-ml fractions. Lane M: Precision Plus Protein™ Standards (Bio-Rad, USA). (C) Coomassie blue-stained 12% SDS-PAGE gel of the final recombinant protein used for crystallization. (D) A crystal of apo-*Bs*Fur grown using the microbatch at 295 K. The dimensions of this crystal were around 0.12×0.11×0.13 mm.

was washed with a washing buffer consisting of 20 mM Tris-HCl (pH 8.0), 5% glycerol, 10 mM EDTA, and 50 mM NaCl. *Bs*Fur was eluted with the same buffer containing 300 mM NaCl. The partially purified protein fraction from the Heparin Sepharose^{TM} column was dialyzed against the washing buffer and loaded onto a column packed with 20 ml of Q-Sepharose resin (GE Healthcare). *Bs*Fur was eluted with 0–1 M NaCl gradient in 20 mM Tris-HCl (pH 8.0), 5% glycerol, and 10 mM EDTA. The eluted fraction containing *Bs*Fur was concentrated and loaded onto a Superdex 75 HR 16/60 column (GE Healthcare) pre-equilibrated with the washing buffer. The *Bs*Fur protein was eluted at ~45 min, with a flow rate of 1 ml/min (Fig. 1A). Crystals of *Bs*Fur were grown at 295 K by using the microbatch crystallization method. Small drops containing 1 µl of the protein solution and an equal volume of a precipitant solution were pipetted under a layer of a 1:1 mixture of silicon oil and paraffin oil in a 72-well HLA plate (Nunc, Denmark).

Data collection

The *Bs*Fur crystals were transferred to a cryoprotectant solution (0.4 M NaH_2PO_4, 1.6 M K_2HPO_4, 0.1 M imidazole; pH 8.0, 0.2 M NaCl, and 20% ethylene glycol) and flash-cooled in a stream of liquid nitrogen at 100 K. Diffraction data were collected using ADSC Quantum 270 detector system at beamline 17A (Photon Factory, Japan). A total of 360 frames (oscillation=1°) were measured with the crystal-to-detector distance set to 250 mm. The exposure time to synchrotron radiation was 2 sec/frame.

Data processing and phasing

The raw data sets were indexed, integrated, and scaled with *HKL2000* program suite (Otwinowski and Minor, 1997). Experimental phasing was performed with the *AutoSol* program (Terwilliger *et al*., 2009) in the *PHENIX* suite (Adams *et al*., 2010), which is an experimental phasing pipeline that combines *HySS* (Hybrid Substructure Search) (Grosse-Kunstleve and Adams, 2003) for finding heavy-atom sites, *Phaser* (McCoy *et al*., 2007) or *SOLVE* (Terwilliger, 2002) for calculating experimental phases, and *RESOLVE* (Terwilliger, 2003) for improved density modification and model building. The auto-built models from the phasing programs were completed using *COOT* (Emsley and Cowtan, 2004) and refinement was performed with a maximum-likelihood algorithm implemented in *CNS* (Brunger *et al*., 1998) or *REFMAC5* (Nicholls *et al*., 2012).

Results and Discussion

Crystallization of *Bs*Fur

The recombinant *Bs*Fur protein containing four cysteine residues in the two Cys-X-X-Cys motifs was successfully cloned, expressed, and purified. Estimation of molecular mass, based on the elution time in size-exclusion chromatography, indicated that the recombinant *Bs*Fur protein exists as a dimer in solution (Fig. 1A). SDS-PAGE analyses show that *Bs*Fur was purified to >90% homogeneity, with a yield of 6 mg protein/L of culture solution (Figs. 1B and 1C). For crystallization, *Bs*Fur was concentrated to approximately 12 mg/ml (Fig. 1C) and initial crystallization trials were performed using commercially available crystallization solutions from Hampton Research, Axygen Biosciences, Emerald BioSystems, KeraFast, Moleculardimensions, and Microlytic, USA. Fortunately, single crystals (0.12×0.11×0.13 mm; Fig. 1D) grew in a precipitant solution containing 0.4 M NaH_2PO_4, 1.6 M K_2HPO_4, 0.1 M imidazole (pH 8.0), and 0.2 M NaCl (condition No. 20 of Wizard I^{TM}; Emerald BioSystems) in 24 h. These initial crystals were used for data collection without further optimization.

Experimental phasing

In Fur family proteins, the C-site, consisting of four cysteine residues, is occupied by zinc, even in the presence of chelating agents that empty the M- and D-sites (Lee and Helmann, 2006; Ma *et al*., 2011, 2012). Therefore, we safely assumed that the C-site would be occupied by zinc in the recombinant *Bs*Fur protein, despite the use of EDTA during purification. After mounting a crystal using a 50-µm MicroMount polmer loop (MiTeGen, USA), a fluorescence scan was performed. Thereafter, a SAD data set (resolution, 2.6 Å) was collected at the zinc absorption peak (λ=1.2823 Å) because experimental phasing using zinc anomalous scattering is considered efficient (Cha *et al*., 2012). The <*d″*/sig> value, which is a good indicator of the strength of the anomalous signal, indicates that the SAD data are adequate for phase determination. The *Bs*Fur crystal belonged to the primitive trigonal space group,

Table 1. Data collection and phasing statistics

Data collection	SAD
Space group	$P3_221$
Beamline	BL-17A; Photon Factory, Japan
Wavelength (Å)	1.28230
Oscillation (°)	360
Unit cell parameters (Å)	$a = b = 57.140$, $c = 109.570$
Resolution (Å)[a]	50-2.60 (2.64-2.60)
Completeness (%)[a]	93.6 (85.7)
R_{merge} (%)[a,b]	7.4 (54.8)
$I/\sigma(I)$[a]	25.0 (4.8)
Multiplicity[a]	20.3 (20.0)
<*d″*/*sig*> of outer shell[c]	0.68
Phasing statistics	
No. of atoms	
Zinc	1
Sulfur	4
Sites occupancies[d]	1.00
FOM[d]	
Before DM	0.45
After DM	0.84
Model-map CC[d]	0.63
R_{work}[e]/R_{free}[f] (%)	0.3052/0.3593

[a] The number enclosed in parentheses is for the outer shell.
[b] $R_{merge} = \Sigma_{hkl} \Sigma_i |I_i(hkl) - \langle I(hkl)\rangle| / \Sigma_{hkl} \Sigma_i I_i(hkl)$, where $I_i(hkl)$ is the intensity of observed reflection *hkl* and $\langle I(hkl)\rangle$ is the mean intensity of symmetry-equivalent reflections.
[c] Data from *SHELXC* (Sheldrick, 2010).
[d] Data from phasing programs.
[e] $R_{work} = \Sigma_{hkl} |F_{obs} - F_{cacl}| / \Sigma_{hkl} |F_{obs}|$, where F_{cacl} and F_{obs} are the calculated and observed structure factors, respectively.
[f] R_{free} is the same as R_{work}, but is calculated for randomly chosen sample (5% of reflections that were omitted from the refinement).

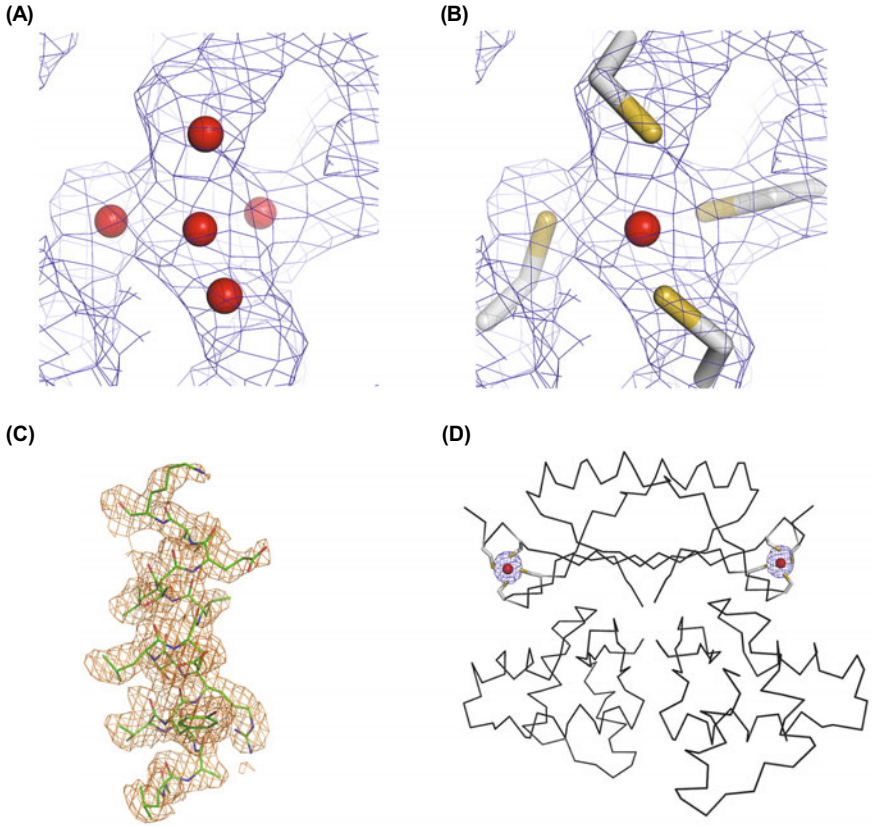

Fig. 2. Representative experimental electron density maps and anomalous Fourier map. (A) Experimental map after density modification contoured at 1σ showing the C-site. Green spheres represent the position of anomalous scatter found by the phasing program. (B) Experimental map after density modification contoured at 1σ superposed onto the C-site in the final model. The red sphere represents a zinc atom, and the cysteine residues that coordinate the zinc atom are represented as sticks. The positions of zinc and sulfur atoms are identical to the positions of anomalous scatters in Fig. 2A. (C) Experimental map after density modification contoured at 1σ showing a helical region in the final model. (D) Anomalous Fourier map at the 5σ level superimposed onto the final apo-*Bs*Fur dimer represented by Cα tracing. The red sphere represents a zinc atom at C-site, and the cysteine residues that coordinate the zinc atom are represented as sticks.

$P3_22_1$ or $P3_12_1$, with the unit cell parameters a =b =57.14, c =109.57 Å (Table 1). The crystal volume per unit molecular weight (V_M) was about 2.99 Å^3 Da^{-1}, with a solvent content of 58.92%, assuming that the asymmetric unit contained one molecule.

Experimental SAD phasing was performed using the *AutoSol* program and one zinc substructure was expected to be present in the asymmetric unit. However, when the space group was set to $P3_22_1$, the program found five zinc substructures (Fig. 2A) and produced a phase set with a figure of merit (FOM) of 0.45 and 0.84 before and after density modification, respectively. The experimental electron-density map was clearly interpretable and a model with a R_{work}/R_{free} of 0.3052/0.3593 was automatically built (Fig. 2C). The identification of five zinc substructures was not compatible with the three metal sites in the monomer of *Bs*Fur and the use of EDTA in purification. Therefore, we examined the location of five zinc substructures with the auto-built model. One zinc substructure represents the expected zinc atom at C-site, whereas the other four turned out to be the ordered sulfur atom positions from the four cysteine residues that coordinate the C-site zinc atom (Figs. 2B and 2D). When the phases were recalculated after eliminating the sulfur atom sites, experimental phasing failed, indicating that our SAD data evidently contained a meaningful anomalous scattering contribution originating from the sulfur atoms. Sulfur has significantly lower anomalous signal (f''=0.39) than zinc (f''=3.89) at the zinc absorption peak. Nevertheless, the high multiplicity of the SAD data (Table 1) and the location of zinc atom, the strong anomalous scatterer, probably led to measuring the poor anomalous signal of sulfur atoms. It is worthwhile to note that the location of the zinc atom facilitates detection of sulfur atoms and the anomalous scattering of sulfur atoms contributes to SAD phasing (Ramagopal *et al.*, 2003; Kim *et al.*, 2013). In conclusion, the successful SAD phasing clearly reveals that the *Bs*Fur protein used in this study has empty M- and D-sites, with its C-site occupied by zinc atom. The final structure of apo-*Bs*Fur shall be described in a future publication.

Acknowledgements

This work was supported by the National Research Foundation of Korea Grant NRF-2012R1A2A2A02005978, the CAP through Korea Research Council of Fundamental Science Technology (KRCF), Korea Institute of Science and Technology (KIST), & Korea Institute of Ocean Science and Technology (KIOST), the Marine and Extreme Genome Research Center program, and the Development of Biohydrogen Production Technology Using Hyperthermophilic Archaea program of MOF. Works performed at Hanyang University were supported by the National Research Foundation of Korea Grant KRF-2008-313-C0077.

References

Adams, P.D., Afonine, P.V., Bunkoczi, G., Chen, V.B., Davis, I.W., Echols, N., Headd, J.J., Hung, L.W., Kapral, G.J., Grosse-Kun-

stleve, R.W., and *et al.* 2010. Phenix: A comprehensive python-based system for macromolecular structure solution. *Acta Crystallogr. D Biol. Crystallogr.* **66**, 213–221.

Berg, J.M. and Shi, Y. 1996. The galvanization of biology: A growing appreciation for the roles of zinc. *Science* **271**, 1081–1085.

Brünger, A.T., Adams, P.D., Clore, G.M., DeLano, W.L., Gros, P., Grosse-Kunstleve, R.W., Jiang, J.S., Kuszewski, J., Nilges, M., Pannu, N.S., and *et al.* 1998. *Crystallography & NMR System*: A new software suite for macromolecular structure determination. *Acta Crystallogr. D Biol. Crystallogr.* **54**, 905–921.

Butcher, J., Sarvan, S., Brunzelle, J.S., Couture, J.F., and Stintzi, A. 2012. Structure and regulon of *Campylobacter jejuni* ferric uptake regulator Fur define apo-Fur regulation. *Proc. Natl. Acad. Sci. USA* **109**, 10047–10052.

Cha, S.S., An, Y.J., Jeong, C.S., Kim, M.K., Lee, S.G., Lee, K.H., and Oh, B.H. 2012. Experimental phasing using zinc anomalous scattering. *Acta Crystallogr. D Biol. Crystallogr.* **68**, 1253–1258.

da Silva Neto, J.F., Braz, V.S., Italiani, V.C., and Marques, M.V. 2009. Fur controls iron homeostasis and oxidative stress defense in the oligotrophic α-Proteobacterium *Caulobacter crescentus*. *Nucleic Acids Res.* **37**, 4812–4825.

Delany, I., Pacheco, A.B., Spohn, G., Rappuoli, R., and Scarlato, V. 2001a. Iron-dependent transcription of the *frpb* gene of *Helicobacter pylori* is controlled by the Fur repressor protein. *J. Bacteriol.* **183**, 4932–4937.

Delany, I., Spohn, G., Rappuoli, R., and Scarlato, V. 2001b. The Fur repressor controls transcription of iron-activated and -repressed genes in *Helicobacter pylori*. *Mol. Microbiol.* **42**, 1297–1309.

Dian, C., Vitale, S., Leonard, G.A., Bahlawane, C., Fauquant, C., Leduc, D., Muller, C., de Reuse, H., Michaud-Soret, I., and Terradot, L. 2011. The structure of the *Helicobacter pylori* ferric uptake regulator Fur reveals three functional metal binding sites. *Mol. Microbiol.* **79**, 1260–1275.

Emsley, P. and Cowtan, K. 2004. *Coot*: model-building tools for molecular graphics. *Acta Crystallogr. D Biol. Crystallogr.* **60**, 2126–2132.

Escolar, L., Perez-Martin, J., and de Lorenzo, V. 1999. Opening the iron box: Transcriptional metalloregulation by the Fur protein. *J. Bacteriol.* **181**, 6223–6229.

Gancz, H., Censini, S., and Merrell, D.S. 2006. Iron and pH homeostasis intersect at the level of Fur regulation in the gastric pathogen *Helicobacter pylori*. *Infect. Immun.* **74**, 602–614.

Grosse-Kunstleve, R.W. and Adams, P.D. 2003. Substructure search procedures for macromolecular structures. *Acta Crystallogr. D Biol. Crystallogr.* **59**, 1966–1973.

Haber, F. and Weiss, J. 1932. On the catalysis of dydroperoxide. *Naturwissenschaften* **20**, 948–950.

Hernandez, J.A., Bes, M.T., Fillat, M.F., Neira, J.L., and Peleato, M.L. 2002. Biochemical analysis of the recombinant Fur (ferric uptake regulator) protein from *Anabaena* PCC 7119: factors affecting its oligomerization state. *Biochem. J.* **366**, 315–322.

Kadner, R.J. 2005. Regulation by iron: RNA rules the rust. *J. Bacteriol.* **187**, 6870–6873.

Kim, M.K., Lee, S., An, Y.J., Jeong, C.S., Ji, C.J., Lee, J.W., and Cha, S.S. 2013. In-house zinc SAD phasing at Cu *k*α edge. *Mol. Cells* **36**, 74–81.

Lee, H.J., Bang, S.H., Lee, K.H., and Park, S.J. 2007. Positive regulation of *fur* gene expression via direct interaction of Fur in a pathogenic bacterium, *Vibrio vulnificus*. *J. Bacteriol.* **189**, 2629–2636.

Lee, J.W. and Helmann, J.D. 2006. Biochemical characterization of the structural Zn^{2+} site in the *Bacillus subtilis* peroxide sensor PerR. *J. Biol. Chem.* **281**, 23567–23578.

Lee, J.W. and Helmann, J.D. 2007. Functional specialization within the Fur family of metalloregulators. *Biometals* **20**, 485–499.

Ma, Z., Faulkner, M.J., and Helmann, J.D. 2012. Origins of specificity and cross-talk in metal ion sensing by *Bacillus subtilis* Fur. *Mol. Microbiol.* **86**, 1144–1155.

Ma, Z., Gabriel, S.E., and Helmann, J.D. 2011. Sequential binding and sensing of Zn(ii) by *Bacillus subtilis* Zur. *Nucleic Acids Res.* **39**, 9130–9138.

McCoy, A.J., Grosse-Kunstleve, R.W., Adams, P.D., Winn, M.D., Storoni, L.C., and Read, R.J. 2007. Phaser crystallographic software. *J. Appl. Crystallogr.* **40**, 658–674.

McHugh, J.P., Rodriguez-Quinones, F., Abdul-Tehrani, H., Svistunenko, D.A., Poole, R.K., Cooper, C.E., and Andrews, S.C. 2003. Global iron-dependent gene regulation in *Escherichia coli*. A new mechanism for iron homeostasis. *J. Biol. Chem.* **278**, 29478–29486.

Nicholls, R.A., Long, F., and Murshudov, G.N. 2012. Low-resolution refinement tools in 5 *Acta Crystallogr. D Biol. Crystallogr.* **68**, 404–417.

Otwinowski, Z. and Minor, W. 1997. Processing of x-ray diffraction data collected in oscillation mode. *Method Enzymol.* **276**, 307–326.

Palyada, K., Threadgill, D., and Stintzi, A. 2004. Iron acquisition and regulation in *Campylobacter jejuni*. *J. Bacteriol.* **186**, 4714–4729.

Pohl, E., Haller, J.C., Mijovilovich, A., Meyer-Klaucke, W., Garman, E., and Vasil, M.L. 2003. Architecture of a protein central to iron homeostasis: Crystal structure and spectroscopic analysis of the ferric uptake regulator. *Mol. Microbiol.* **47**, 903–915.

Ramagopal, U.A., Dauter, M., and Dauter, Z. 2003. Phasing on anomalous signal of sulfurs: What is the limit? *Acta Crystallogr. D Biol. Crystallogr.* **59**, 1020–1027.

Schaible, U.E. and Kaufmann, S.H. 2004. Iron and microbial infection. *Nat. Rev. Microbiol.* **2**, 946–953.

Sheikh, M.A. and Taylor, G.L. 2009. Crystal structure of the *Vibrio cholerae* ferric uptake regulator (Fur) reveals insights into metal co-ordination. *Mol. Microbiol.* **72**, 1208–1220.

Sheldrick, G.M. 2010. Experimental phasing with shelxc/d/e: Combining chain tracing with density modification. *Acta Crystallogr. D Biol. Crystallogr.* **66**, 479–485.

Shin, J.H., Jung, H.J., An, Y.J., Cho, Y.B., Cha, S.S., and Roe, J.H. 2011. Graded expression of zinc-responsive genes through two regulatory zinc-binding sites in Zur. *Proc. Natl. Acad. Sci. USA* **108**, 5045–5050.

Terwilliger, T.C. 2002. Automated structure solution, density modification and model building. *Acta Crystallogr. D Biol. Crystallogr.* **58**, 1937–1940.

Terwilliger, T.C. 2003. Solve and resolve: Automated structure solution and density modification. *Methods Enzymol.* **374**, 22–37.

Terwilliger, T.C., Adams, P.D., Read, R.J., McCoy, A.J., Moriarty, N.W., Grosse-Kunstleve, R.W., Afonine, P.V., Zwart, P.H., and Hung, L.W. 2009. Decision-making in structure solution using Bayesian estimates of map quality: The PHENIX AutoSol wizard. *Acta Crystallogr. D Biol. Crystallogr.* **65**, 582–601.

Torres, V.J., Attia, A.S., Mason, W.J., Hood, M.I., Corbin, B.D., Beasley, F.C., Anderson, K.L., Stauff, D.L., McDonald, W.H., Zimmerman, L.J., and *et al.* 2010. *Staphylococcus aureus* fur regulates the expression of virulence factors that contribute to the pathogenesis of pneumonia. *Infect. Immun.* **78**, 1618–1628.

Traore, D.A., El Ghazouani, A., Ilango, S., Dupuy, J., Jacquamet, L., Ferrer, J.L., Caux-Thang, C., Duarte, V., and Latour, J.M. 2006. Crystal structure of the apo-PerR-Zn protein from *Bacillus subtilis*. *Mol. Microbiol.* **61**, 1211–1219.